CrossMark

J. Fluid Mech. (2016), *vol.* 793, *pp.* 21–40. © Cambridge University Press 2016
doi:10.1017/jfm.2016.124

Buoyancy effects in a wall jet over a heated horizontal plate

R. Fernandez-Feria[1],† and F. Castillo-Carrasco[1]

[1]Universidad de Málaga, Andalucía Tech, E. T. S. Ingeniería Industrial, Dr Ortiz Ramos s/n, 29071 Málaga, Spain

(Received 16 October 2015; revised 15 December 2015; accepted 10 February 2016; first published online 15 March 2016)

A similarity solution of the boundary layer equations for a wall jet on a heated horizontal surface at constant temperature taking into account the coupling of the temperature and velocity fields by buoyancy is described. This similarity solution exists for any value of $\Lambda = Gr/Re^2$, characterizing this coupling between natural and forced convection over the horizontal plate, where Gr is a Grashof number and Re is a Reynolds number, provided that the plate temperature is higher than the ambient temperature ($\Lambda > 0$, say). Two main qualitative differences are found in the flow structure in relation to the well-known Glauert's similarity solution for a wall jet without natural convection effects (i.e. when $\Lambda = 0$): the first is that the similarity variable and structure of the horizontal velocity and temperature have the same functional form for both a radially spreading jet and a two-dimensional jet; the second is that the maximum of the horizontal velocity increases as the jet spreads over the surface, instead of decreasing like in Glauert's solution, as the radial or horizontal distance to the power $1/5$. To check this similarity solution we solve numerically the boundary layer equations for the particular case of a jet with constant velocity and temperature emerging from a slot of height δ and radius r_0 (in the radially spreading case). An approximate, analytical similarity solution near the jet exit is also found that helps to start the numerical integration. Far from the jet exit the numerical solution tends to the similarity solution for any set of values of the non-dimensional parameters governing the problem, provided that the plate is heated ($\Lambda > 0$). No similarity solution is found numerically for the case of a cooled plate ($\Lambda < 0$). For $\Lambda = 0$ Glauert's similarity solution is recovered.

Key words: boundary layer structure, buoyant boundary layers, jets

1. Introduction

It is well known that a jet spreading, either radially or in two dimensions, over a plate surface may be described by a similarity solution of the laminar boundary layer equations when the Reynolds number is sufficiently high (Glauert 1956). If the temperature of the horizontal plate is different from the ambient temperature, and also from the temperature of the emerging jet, buoyancy forces may be relevant, coupling the temperature and the velocity fields of the flow over the plate. Mixed-convection

† Email address for correspondence: ramon.fernandez@uma.es

https://doi.org/10.1017/jfm.2016.124 Published online by Cambridge University Press

problems over a horizontal plate have been widely studied in the past due to their engineering, as well as theoretical, interest. For instance, for a constant external velocity above the plate, the problem has a similarity solution for specific power-law temperature distributions on the horizontal plate (Sparrow, Eichhorn & Gregg 1959; Gill & del Casal 1962; Leal 1973; Schneider 1979; Afzal & Hussain 1984; Denier, Duck & Li 2005; Deswita *et al.* 2010), but not for the case of a constant temperature plate. The solutions for the cases of an insulated and of a cooled horizontal plate present some interesting features, such as singularity and non-uniqueness (Schneider & Wasel 1985; Daniels 1992; Daniels & Gargaro 1993; Steinrück 1994, 1995; Higuera 1997; Denier *et al.* 2005), which are not found for the case of the flow over a heated horizontal plate at constant temperature (Fernandez-Feria, del Pino & Fernandez-Gutierrez 2014). In particular, for an insulated plate, a similarity solution exists provided that the local Froude number, measuring the importance of inertia relative to buoyancy, is above a threshold value. Below this value the boundary layer approximation fails either by the onset of reverse flow or more generally by the occurrence of a terminal singularity associated with a sudden rise in skin friction (Daniels 1992; Daniels & Gargaro 1993). On the other hand, flow separation from the wall occurs for sufficiently small Froude numbers in the case of a two-dimensional jet over a cooled plate (Higuera 1997), or in the case of a radial flow above a heated plate when the Grashof number based on the radius of the issued external velocity is sufficiently small (Fernandez-Feria *et al.* 2014).

We consider here the case of a vanishing external velocity far above the plate, i.e. the case of a wall jet spreading radially or in two dimensions, but taking into account the coupling of the temperature and velocity fields by buoyancy when the plate temperature remains constant and higher than the ambient temperature. We show that this problem, when governed by a boundary layer approximation for a sufficiently high Reynolds number, has a far-field similarity solution valid for both the radial flow and the two-dimensional flow. The wall jet structure described by this similarity solution is radically different from Glauert's (1956) similarity solution without buoyancy forces, and qualitatively different (although mathematically equivalent in the two-dimensional case) from Stewartson's (1958) similarity solution for the purely free convection problem over a horizontal surface. To the best of our knowledge, the solution has not been described in the literature.

The similarity solution is obtained in § 3, where it is demonstrated that it exists only for a heated plate for any value of the Froude number (whose inverse is named Λ), but not for a cooled plate. To check numerically the existence of the similarity solution, and to define the different non-dimensional parameters governing the problem, we present first in § 2 a particular problem where a uniform jet with constant velocity and temperature emerges from a slot of height δ and radius r_0 (in the radially spreading case). Both the radial (or axisymmetric) and the two-dimensional problems are formulated together, just differing in the value of an index, to facilitate the comparison of their results. The wall jet in absence of buoyancy forces is also included as the case $\Lambda = 0$. To start the numerical integration of the resulting parabolic, integro-differential equations, we use an approximate similarity solution valid near the jet exit that contains the first-order effect due to the buoyancy forces on the jet (described in appendix A). This solution is also used to validate the numerical method, which is described in § 4. The main numerical results are described and discussed also in § 4, while some conclusions are drawn in § 5.

https://doi.org/10.1017/jfm.2016.124 Published online by Cambridge University Press

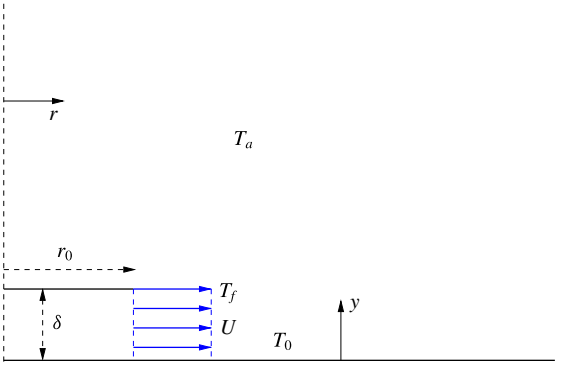


FIGURE 1. (Colour online) Schematic of the problem (with dimensional variables and parameters).

2. Formulation of the problem

We consider in this section a planar jet flow spreading over a horizontal plate, which is set at a constant temperature T_0 higher than the ambient temperature T_a, of a fluid emerging radially with uniform velocity U and temperature $T_f \leqslant T_0$ from a circular slot of radius r_0 and height δ (see figure 1; in the two-dimensional case, the uniform jet emerges from $r = 0$). Assuming that the Reynolds number based on U and δ is sufficiently large,

$$Re = \frac{U\delta}{\nu} \gg 1, \tag{2.1}$$

where ν is the kinematic viscosity of the fluid at the reference temperature T_a, a boundary layer approximation can be used. Assuming also axisymmetry of the flow, scaling the horizontal coordinate r with $L \equiv \delta^2 U/\nu$, the vertical coordinate y with δ, the horizontal velocity component u with U, the vertical velocity component v with $U\,Re^{-1} = U\delta/L$, and using the Boussinesq approximation to model the buoyancy effects induced by the temperature difference, with non-dimensional temperature defined as $\theta = (T - T_a)/(T_0 - T_a)$, the governing non-dimensional (continuity, momentum and energy) equations can be written as (Fernandez-Feria *et al.* 2014)

$$\frac{1}{r^j}\frac{\partial}{\partial r}(r^j u) + \frac{\partial v}{\partial y} = 0, \tag{2.2}$$

$$u\frac{\partial u}{\partial r} + v\frac{\partial u}{\partial y} - \frac{\partial^2 u}{\partial y^2} = \Lambda\frac{\partial}{\partial r}\int_y^\infty \theta\,\mathrm{d}y, \tag{2.3}$$

$$u\frac{\partial \theta}{\partial r} + v\frac{\partial \theta}{\partial y} = \frac{1}{Pr}\frac{\partial^2 \theta}{\partial y^2}, \tag{2.4}$$

where

$$Pr = \frac{\nu}{\alpha} \quad \text{and} \quad \Lambda = \frac{\beta g \delta (T_0 - T_a)}{U^2} = \frac{Gr}{Re^2} \tag{2.5a,b}$$

are the Prandtl number and a non-dimensional parameter related to the Grashof (Gr) and Reynolds numbers, respectively, with α and β the thermal diffusivity and thermal expansivity of the fluid at the reference temperature T_a, respectively, and g the acceleration due to gravity ($\beta = 1/T_a$ for an ideal gas). An index j has been used in

https://doi.org/10.1017/jfm.2016.124 Published online by Cambridge University Press

(2.2) to include in the same formulation the axisymmetric radial flow, corresponding to $j=1$, and the two-dimensional (2D) flow, corresponding to $j=0$, so that one may easily compare the results from both configurations. Note that the last term in the horizontal momentum equation (2.3) represents the pressure gradient due to buoyancy forces induced by the temperature difference when the Boussinesq approximation is used. It is written here as an integro-differential term once the horizontal pressure gradient is transformed by using the vertical momentum equation,

$$0=-\frac{\partial p}{\partial y}+\Lambda\theta, \tag{2.6}$$

where the relative pressure p is scaled with $\rho_a U^2$, with ρ_a the fluid density at ambient temperature, after eliminating the pressure by cross-differentiation of the horizontal and the vertical momentum equations, and integrating the resulting equation across the boundary layer:

$$u\frac{\partial u}{\partial r}+v\frac{\partial u}{\partial y}=\frac{\partial^2 u}{\partial y^2}-\left.\frac{\partial^2 u}{\partial y^2}\right|_{y=0}-\Lambda\frac{\partial}{\partial r}\int_0^y\theta\,\mathrm{d}y, \tag{2.7}$$

$$\left.\frac{\partial^2 u}{\partial y^2}\right|_{y=0}=\left.\frac{\partial p}{\partial r}\right|_{y=0}=-\Lambda\frac{\partial}{\partial r}\int_0^\infty\theta\,\mathrm{d}y. \tag{2.8}$$

This coupling of the temperature and velocity fields by buoyancy is characterized by the non-dimensional parameter Λ, which is akin to the inverse of a Froude number (Daniels 1992; Higuera 1997).

The boundary conditions can be written as

$$u=v=0,\quad \theta=1\quad \text{at } y=0, \tag{2.9a,b}$$

$$u=\theta=0\quad \text{as } y\to\infty, \tag{2.10}$$

$$u=\begin{cases}1, & y\leqslant 1\\ 0, & y>1,\end{cases}\qquad \theta=\begin{cases}\theta_f, & y\leqslant 1\\ 0, & y>1\end{cases}\quad \text{at } r=jR_0, \tag{2.11a,b}$$

where

$$\theta_f=\frac{T_f-T_a}{T_0-T_a},\qquad R_0=\frac{r_0}{L}=\frac{1}{Re}\frac{r_0}{\delta}. \tag{2.12a,b}$$

The problem is thus governed by four non-dimensional parameters: Pr, Λ, θ_f and R_0. In the 2D flow ($j=0$), the last one disappears. θ_f also vanishes in the particular case in which the fluid enters at the ambient temperature ($T_f=T_a$). Finally, $\Lambda=0$ corresponds to the case without thermal or natural convection effects, i.e. the classical wall jet considered by Glauert (1956).

3. Similarity solution far from the jet exit

To integrate numerically (2.2)–(2.11) one may start from a self-similar solution valid near the jet exit, i.e. for $\zeta\equiv r-jR_0\ll 1$, given in appendix A. This will be done in § 4 for several significant values of the non-dimensional parameters. But, before that, it is of interest to search for a more general similarity solution of the problem valid in the opposite limit far from the jet exit, $r\gg\max(1,jR_0)$. Then we shall compare its structure, if such solution exists, with the numerical solution.

https://doi.org/10.1017/jfm.2016.124 Published online by Cambridge University Press

Defining the non-dimensional stream function ψ as

$$u = \frac{1}{r^j}\frac{\partial \psi}{\partial y}, \quad v = -\frac{1}{r^j}\frac{\partial \psi}{\partial r}, \tag{3.1a,b}$$

in terms of which the continuity equation (2.2) is identically satisfied, we look for solutions of (2.3)–(2.4) in the form

$$\psi = Ar^a f(\tau), \quad \theta = Cr^c g(\tau), \quad \tau = B\frac{y}{r^b}, \tag{3.2a–c}$$

where a, b and c are constants, compatible with the boundary conditions (2.9)–(2.10), but disregarding the 'initial' condition (2.11*a*,*b*). Constants A, B and C are selected to eliminate from the resulting similarity problem as many parameters as possible. Clearly,

$$c = 0 \quad \text{and} \quad C = 1 \tag{3.3a,b}$$

to satisfy the temperature boundary condition at the wall $g(\tau = 0) = 1$. From (3.1) and (3.2),

$$u = ABr^{a-b-j}f', \quad v = -Ar^{a-1-j}(af - b\tau f'), \tag{3.4a,b}$$

where the primes denote differentiation with respect to τ. Substituting into (2.3)–(2.10) one gets

$$\frac{1}{5}f'^2 - \left(j + \frac{3}{5}\right)ff'' - f''' = \tau g + \int_\tau^\infty g\,\mathrm{d}\tau, \tag{3.5}$$

$$g'' + Pr(j + \tfrac{3}{5})fg' = 0, \tag{3.6}$$

$$f(0) = f'(0) = f'(\infty) = g(\infty) = 0, \quad g(0) = 1, \tag{3.7a,b}$$

with

$$a = j + \frac{3}{5}, \quad b = \frac{2}{5}, \quad A = B = \left(\frac{2\Lambda}{5}\right)^{1/5}. \tag{3.8a–c}$$

This selection of A and B eliminates the non-dimensional parameter Λ from the problem (3.5)–(3.7), which thus only depends on Pr and j, so that the similarity solutions contains explicitly its dependence on Λ (see below). Curiously, the similarity variable τ is the same in both the 2D and the axisymmetric cases ($j = 0$ and 1),

$$\tau = \left(\frac{2\Lambda}{5}\right)^{1/5}\frac{y}{r^{2/5}}, \tag{3.9}$$

and so is the horizontal or radial dependence of u,

$$u = \left(\frac{2\Lambda}{5}\right)^{2/5} r^{1/5} f'(\tau). \tag{3.10}$$

This contrasts Glauert's (1956) similarity solution for the case without buoyancy forces, whose horizontal variation depends on j: in our notation, $u \sim r^{-(j+1/2)}f_G'(\tau_G)$, where $\tau_G \sim y/r^{(j+3/2)/2}$ (see § 4.2 below for more details) and f_G satisfies equation (4.1) in Glauert (1956),

$$2f_G'^2 + f_G f_G' + f_G''' = 0, \quad f_G(0) = f_G'(0) = f_G'(\infty) = 0. \tag{3.11a,b}$$

https://doi.org/10.1017/jfm.2016.124 Published online by Cambridge University Press

In the present similarity solution, only the vertical velocity v depends explicitly on the radial divergence of the flow,

$$v = -\left(\frac{2\Lambda}{5}\right)^{1/5} r^{-2/5}\left[\left(j+\frac{3}{5}\right)f - \frac{2}{5}\tau f'\right], \tag{3.12}$$

although both functions f and g depend on j through (3.5)–(3.6), in terms of which the non-dimensional stream function and temperature can be written as

$$\psi = \left(\frac{2\Lambda}{5}\right)^{1/5} r^{j+3/5} f(\tau), \quad \theta = g(\tau). \tag{3.13a,b}$$

Note that, according to (3.10), the maximum of u grows slowly with r, while in Glauert's solution the maximum of u decays with r for both $j=0$ and $j=1$ (see also § 4). The temperature field corresponding to Glauert's solution behaves, for the case of a 2D flow ($j=0$), as $\theta \sim r^{-1/4} g_G(\tau_G)$ (Daniels & Gargaro 1992), whose downstream evolution is also qualitatively very different from that given by (3.13).

It is also worth noticing here that, for $j=0$, the problem (3.5)–(3.7) is mathematically quite similar to the purely free convection problem analysed by Stewartson (1958) (see also Schlichting & Gersten 2000, § 10.6). However, the similarity variables (3.9)–(3.10) and (3.13) are qualitatively different from those of Stewartson because here we have a mixed-convection problem governed by Λ, the inverse of a Froude number, that contains a characteristic horizontal speed U. In addition, only the two-dimensional ($j=0$) flow was considered, while r stands here for the streamwise coordinate in both the 2D flow and the radially spreading flow.

The problem (3.5)–(3.7) has a solution for any value of Pr, for $j=0$ and $j=1$, which can be easily obtained numerically by standard numerical methods. This means that, according to the above similarity variables, a similarity solution far from the jet exit exists for any $\Lambda > 0$, but no solution exists for $\Lambda \leqslant 0$. In fact, for $\Lambda = 0$, the structure of the flow, which corresponds to Glauert's similarity solution, is quite different, as indicated above, while for $\Lambda < 0$, i.e. for a cooled plate, no similarity solution exists at all, in agreement with some previous works referred to in § 1. Figure 2 shows the scaled vertical profiles of the radial velocity, $f'(\tau) = r^{-1/5}(2\Lambda/5)^{-2/5}\,u$, and the temperature, $g(\tau) = \theta$, for $Pr = 0.7$ (e.g. air) in the 2D flow and in the axisymmetric case. The structure of the solutions for other values of Pr is quite similar, with different slopes at the wall $y=0$. In § 4 we shall check that the numerical solution of (2.2)–(2.11a,b) tends to this similarity solution far from the exit provided that $\Lambda > 0$, for any value of j, Pr and θ_f. For $\Lambda = 0$, we shall show that the numerical solution tends to Glauert's similarity solution, which is radically different, as already commented on, while for $\Lambda < 0$ no similarity solution will be reached at all.

Of particular interest are the local skin friction coefficient at the wall and the local Nusselt number (or non-dimensional heat transfer at the wall), whose radial variations and their dependence on Λ are given explicitly from the similarity variables:

$$c_f \equiv \left.\frac{\partial u}{\partial y}\right|_{y=0} = f''(0)\left(\frac{2\Lambda}{5}\right)^{3/5} r^{-1/5}, \tag{3.14}$$

$$Nu \equiv -\left.\frac{\partial \theta}{\partial y}\right|_{y=0} = -g'(0)\left(\frac{2\Lambda}{5}\right)^{1/5} r^{-2/5}. \tag{3.15}$$

https://doi.org/10.1017/jfm.2016.124 Published online by Cambridge University Press

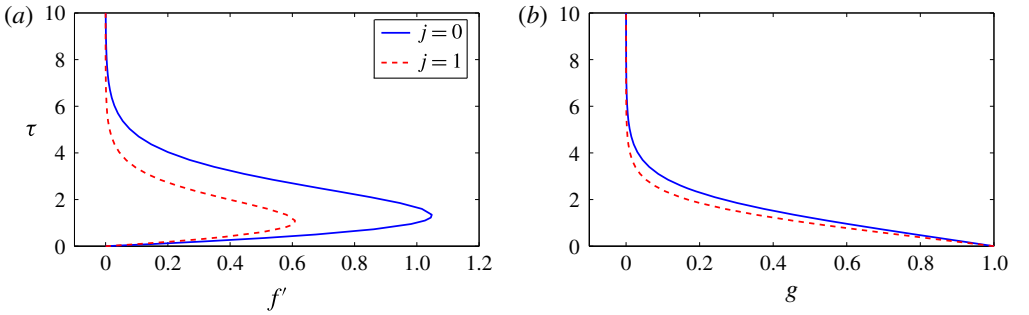


FIGURE 2. (Colour online) $f'(\tau)$ (*a*) and $g(\tau)$ (*b*) from (3.5) to (3.7) for $Pr = 0.7$, for the 2D case ($j = 0$) and the axisymmetric case ($j = 1$).

Also of physical interest is the radial or horizontal pressure gradient, which depends on y due to the buoyancy forces. At the wall, the non-dimensional radial pressure gradient can be written as

$$\left.\frac{\partial p}{\partial r}\right|_{y=0} = -\Lambda \frac{\partial}{\partial r}\int_0^\infty \theta \, \mathrm{d}y = -G(0)\left(\frac{2\Lambda}{5}\right)^{4/5} r^{-3/5}, \tag{3.16}$$

where

$$G(\tau) \equiv \int_\tau^\infty g(\tau)\, \mathrm{d}\tau \geqslant 0. \tag{3.17}$$

Note that the similarity solution is valid only far from the jet exit, so that the singularities as $r \to 0$ in (3.14)–(3.16) are not physically relevant. It is clear that the horizontal pressure gradient at the wall is always negative, i.e. if the present self-similar solution is reached, no adverse pressure gradient is generated in the boundary layer flow, vanishing as $r \to \infty$. The absolute value of the radial pressure gradient at any other height y is always smaller than that at the wall, since the maximum of $G(\tau)$ is reached at $\tau = 0$.

The dependencies on j and on Pr of $f''(0)$, $g'(0)$ and $G(0)$, and, therefore, the variation with j and Pr of c_f, Nu and the pressure gradient, have to be obtained numerically. Actually, the variation with Pr obtained numerically can be fitted to simple power laws very accurately, valid for any Pr in the case of c_f, and for $Pr \lesssim 1$ or $Pr \gtrsim 3$ in the case of Nu and the pressure gradient:

$$f''(0) \simeq \begin{cases} 1.48\, Pr^{-0.38}, & j = 0, \\ 1.04\, Pr^{-0.38}, & j = 1, \end{cases} \quad \text{for any } Pr, \tag{3.18}$$

$$g'(0) \simeq \begin{cases} -0.47\, Pr^{1/3}, & j = 0, \\ -0.62\, Pr^{1/3}, & j = 1, \end{cases} \quad \text{for } Pr \lesssim 1, \tag{3.19}$$

$$g'(0) \simeq \begin{cases} -0.49\, Pr^{0.22}, & j = 0, \\ -0.60\, Pr^{0.22}, & j = 1, \end{cases} \quad \text{for } Pr \gtrsim 3, \tag{3.20}$$

$$G(0) \simeq \begin{cases} 1.25\, Pr^{-0.36}, & j = 0, \\ 1.00\, Pr^{-0.36}, & j = 1, \end{cases} \quad \text{for } Pr \lesssim 1, \tag{3.21}$$

$$G(0) \simeq \begin{cases} 1.23\, Pr^{-0.23}, & j = 0, \\ 1.00\, Pr^{-0.23}, & j = 1, \end{cases} \quad \text{for } Pr \gtrsim 3. \tag{3.22}$$

https://doi.org/10.1017/jfm.2016.124 Published online by Cambridge University Press

Some of these approximations can be refined using the formal integration of (3.6) that provides a general expression for g in terms of f:

$$g = 1 + g'(0) \int_0^\tau \exp\left[-\left(j+\frac{3}{5}\right) Pr \int_0^\tau f \,\mathrm{d}\tau\right] \mathrm{d}\tau, \tag{3.23}$$

where the boundary condition $g(0) = 1$ has been used. On using the other boundary condition for g,

$$g'(0) = -\left\{\int_0^\infty \exp\left[-\left(j+\frac{3}{5}\right) Pr \int_0^\tau f \,\mathrm{d}\tau\right] \mathrm{d}\tau\right\}^{-1}. \tag{3.24}$$

These expressions can be used to obtain the dependencies of $g'(0)$ and $G(0)$ with Pr in the limits $Pr \ll 1$ and $Pr \gg 1$. But, since they depend on $f(\tau)$, which has to be obtained numerically, the procedure has no real advantage from the purely numerical one used above.

It is also of practical interest to write (3.14) and (3.15) in terms of the Grashof number ($Gr = \beta g \delta^3 (T_0 - T_a)/\nu^2$) explicitly:

$$c_f = f''(0) \left(\frac{2}{5}\right)^{3/5} \frac{Gr^{3/5}}{Re} \bar{r}^{-1/5}, \tag{3.25}$$

$$Nu = -g'(0) \left(\frac{2}{5}\right)^{1/5} Gr^{1/5} \bar{r}^{-2/5}, \tag{3.26}$$

where $\bar{r}$ is the non-dimensional radial distance scaled with δ instead of L (i.e. $\bar{r} = Re\, r$). Thus, $Nu \propto Pr^{1/3} Gr^{1/5} \bar{r}^{-2/5}$ for $Pr \lesssim 1$ and $Nu \propto Pr^{0.22} Gr^{1/5} \bar{r}^{-2/5}$ for $Pr \gtrsim 3$, and it does not depend on Re.

4. Numerical results and discussion

4.1. *Numerical method and validation*

To integrate numerically the problem (2.2)–(2.11*a*,*b*) we use a pseudospectral-based method of lines, as described in Fernandez-Feria & Ortega-Casanova (2014). The vertical velocity v is written in terms of u from (2.2) and substituted into (2.3)–(2.4). The resulting integro-differential equations for u and θ are discretized in the vertical direction using a Chebyshev pseudospectral collocation method. Then, the set of ordinary differential equations on the collocation points is integrated in the radial direction using an accurate method of lines, starting from the approximate similarity solution described in appendix A at a given $r_{in} = \zeta_{in} + jR_0$, with $\zeta_{in} \ll 1$ and $\zeta_{in} \ll R_0$ (if $j = 1$).

To discretize the equations along the vertical direction we concentrate the collocation nodes near the plate $y = 0$ and near $y = 1$, where the velocity gradients are very large close to the jet exit. To that end we use the following transformations to map the Chebyshev collocation points $s_i = \cos(\mathrm{i}\pi/N)$, $i = 0, 1, \ldots, N$, defined in the interval $[-1, 1]$, into the computational nodes y_i in the domain $[0, \infty)$:

$$t_i = \frac{a(1+s_i)}{2a/t_M + 1 - s_i}, \quad y_i = a_0 \frac{1 - \mathrm{e}^{-mt_i}}{b_0 + \mathrm{e}^{-mt_i}} + c_0 t_i \mathrm{e}^{t_i/t_M - 1}, \quad i = 0, 1, \ldots, N. \tag{4.1a,b}$$

The first transformation maps the interval $[-1, 1]$ onto $[0, t_M]$, where $t_M \gg 1$ is related to the point $y_M \gg 1$ (see below) at which the boundary conditions as $y \to \infty$

https://doi.org/10.1017/jfm.2016.124 Published online by Cambridge University Press

are imposed. Approximately half the nodes are in $0 \leqslant t \leqslant a$, thus concentrating the nodes near the plate (we choose $a = 2$ and $t_M = 1000$ in all the reported computations). The second transformation, mapping $0 \leqslant t_i \leqslant t_M$ onto $0 \leqslant y_i \leqslant y_M$, concentrates the computational nodes near $y = 1$, maintaining their high concentration close to the plate and their sparseness far from the plate. Note that $y_M \approx c_0 t_M$ if a_0/b_0 is order unity ($y_M \simeq 500$ in all the reported computations). The values of the parameters used in all the computations reported below are $a_0 = 0.04$, $b_0 = 0.0548$, $c_0 = 0.5$, $m = 6$, and N between 80 and 200. Note that $i = N$ corresponds to the plate ($y_N = 0$) and $i = 0$ to the point at infinity ($y_0 = y_M$).

In addition to the Chebyshev collocation points with the above transformations we also tried a Laguerre pseudospectral collocation method, since Laguerre collocation points are already distributed in [0, ∞) (Boyd 2000). But, after using the second transformation (4.1) on Laguerre's points to concentrate the nodes near $y = 1$, the method yielded poorer results. The reason was that Laguerre collocation points are not sufficiently packed near $y = 0$ for the same y_M, so that one has to use a much higher number of nodes N than with the above transformations of Cbebyshev's collocation points to obtain the same accuracy near the plate.

Another numerical difficulty, apart from the required node concentration at $y = 0$ and $y = 1$ to start the numerical integration, is the boundary condition of u as $y \to \infty$ (implemented at y_M). Since u tends to zero there, the mass matrix $\boldsymbol{M}$ in the method of lines (Fernandez-Feria & Ortega-Casanova 2014) becomes very ill conditioned or close to singular, depending on y_M and on the number of nodes N. To circumvent this difficulty, we replaced that boundary condition in (2.10) by $u(r, y_M) = \epsilon \ll 1$. In most reported computations we choose $\epsilon = 4 \times 10^{-3}$.

To validate the numerical integration, checking its agreement with the approximate self-similar solution for small ζ given in appendix A, figure 3 shows the vertical profiles of u for the 2D case ($j = 0$) and for the radial case ($j = 1$) with $R_0 = 0.1$, for $\Lambda = 0$ and $\Lambda = 1$. The numerical solutions are obtained starting at $\zeta_i = 3 \times 10^{-4}$ from the self-similar approximation for $\zeta \ll 1$ using $N = 160$ pseudospectral nodes in the vertical direction from $y = 0$ to $y = y_M \simeq 500$, where the boundary conditions as $y \to \infty$ are set, and Matlab's `ode23t` code (with default error tolerance values) to advance in the horizontal direction solving the ordinary differential equations resulting from the method of lines. It is observed that the accuracy of the numerical solutions is quite satisfactory with these numerical parameters, since they practically coincide with the self-similar ones at least up to $\zeta = 0.0048$ in all cases. Actually, the self-similar solution becomes poorer faster as ζ increases in the axisymmetric case due to the radial divergence of the flow, particularly for $\Lambda \neq 0$, an effect that is more important as R_0 decreases. In the 2D case ($j = 0$) with $\Lambda = 0$, the approximate self-similar solution with the two terms given in appendix A remains quite accurate up to $\zeta \sim 0.1$, as is more clearly observed in figure 4(*a*), while for $\Lambda = 1$ and $j = 1$ with $R_0 = 0.1$ (figure 4*d*) the self-similar solution is already quite poor for $\zeta \sim 0.025$. These figures show the horizontal evolutions of the non-dimensional skin friction at the wall (c_f) and heat flux at the wall ($-Nu$, the minus sign is just to separate the curves in the same plot) computed both numerically and with the similarity solution valid for $\zeta = r - jR_0 \ll 1$.

The vertical gradients of the fluid magnitudes (particularly of u and v) are very strong near $y = 0$ and $y = 1$ only close to the jet exit (small ζ). As the flow moves forward the vertical gradients around these points decay very fast, becoming more uniformly distributed along the vertical direction. Therefore, it is not necessary to keep the high node concentrations near these points. For this reason, after the initial

https://doi.org/10.1017/jfm.2016.124 Published online by Cambridge University Press

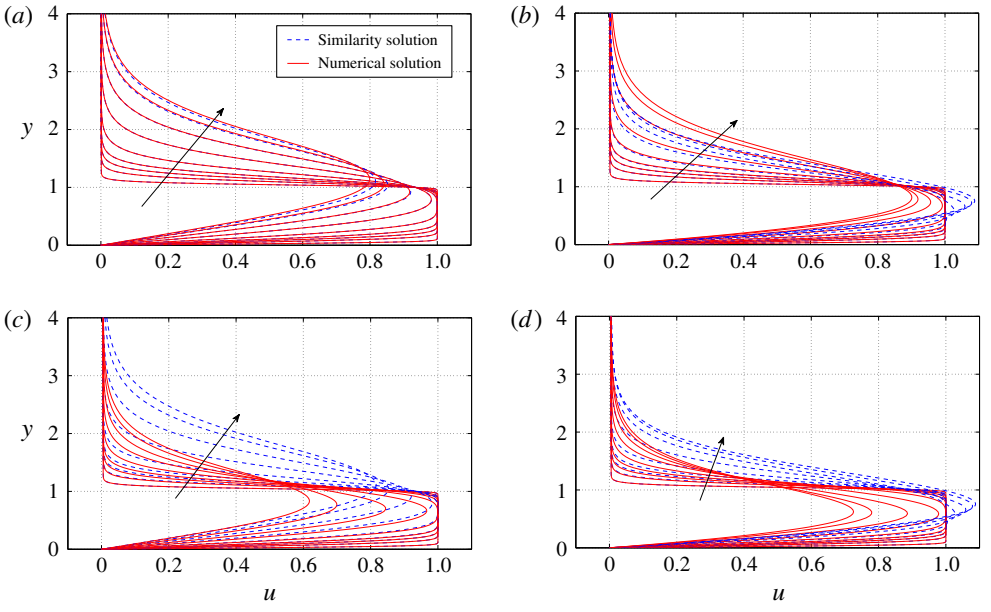


FIGURE 3. (Colour online) Comparison of the vertical profiles of the radial velocity computed numerically with those from the similarity solution valid for $\zeta \ll 1$ for several values of ζ: 0.0003, 0.0014, 0.0028, 0.0048, 0.01, 0.025, 0.05, 0.08, 0.1, increasing in the direction of the arrow. 2D case (a,b) and axisymmetric case with $R_0 = 0.1$ (c,d) for $\Lambda = 0$ (a,c) and $\Lambda = 1$ (b,d). $Pr = 0.7$, $\theta_f = 0$: (a,b) $j = 0$, (c,d) $j = 1$.

numerical difficulties are circumvented with the above-defined transformations, we restarted the numerical integration along r at $\zeta = 5$ using a more uniform node distribution, with just the first transformation in (4.1) with $a = 30$ for $\Lambda \neq 0$ and $a = 50$ for $\Lambda = 0$. All the numerical solutions reported below are computed following this scheme: with a high concentration of nodes both near $y = 0$ and near $y = 1$ up to $\zeta = 5$, and then using a more uniform node distribution from $\zeta = 5$ onwards.

4.2. *Results for* $\Lambda = 0$

As already commented on, for $\Lambda = 0$ with $\theta_f = 0$ the solution must tend, far from the jet exit, to the similarity solution for the velocity field found by Glauert (1956). This is checked here both for the 2D case and the axisymmetric case when $Pr = 0.7$. In our notation, the radial velocity field given by Glauert's similarity solution can be written as

$$u = A_G r^{-(j+1/2)} f_G'(\tau_G), \qquad \tau_G = B_G \frac{y}{r^{(j+3/2)/2}}, \tag{4.2a,b}$$

where f_G satisfies equation (2.7) in (Glauert 1956) and

$$A_G = \begin{cases} \dfrac{1}{4Re}, & j = 0 \\ \dfrac{3}{4Re^3}, & j = 1, \end{cases} \qquad B_G = \begin{cases} \dfrac{1}{4Re^{1/2}}, & j = 0 \\ \dfrac{3}{4Re^{3/2}}, & j = 1. \end{cases} \tag{4.3a,b}$$

The corresponding non-dimensional skin friction at the wall is

$$c_f = A_G B_G f_G''(0) r^{-(3j+5/2)/2}. \tag{4.4}$$

https://doi.org/10.1017/jfm.2016.124 Published online by Cambridge University Press

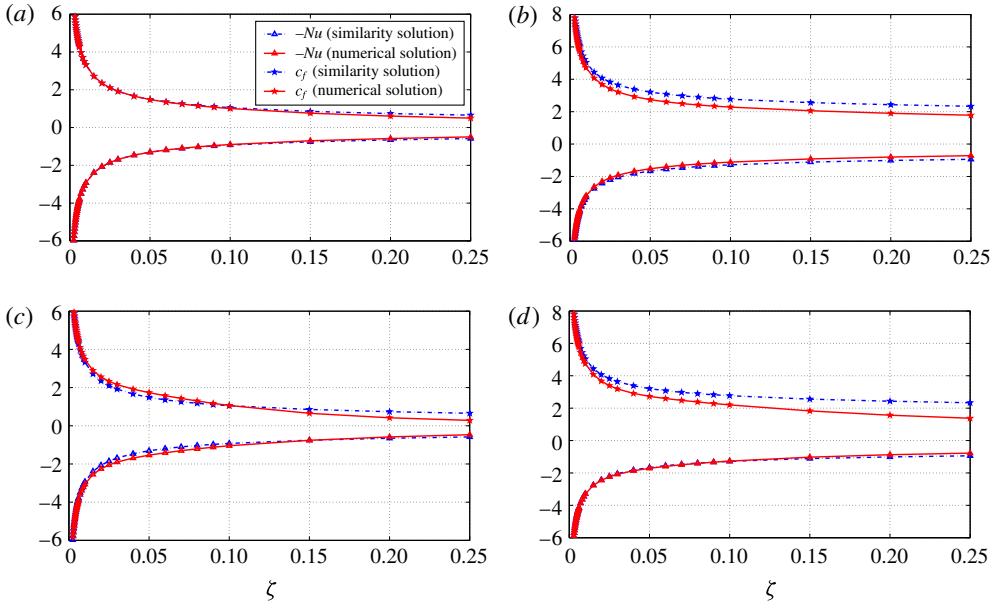


FIGURE 4. (Colour online) Comparison of the radial variation of $-Nu$ and c_f computed numerically with those from the similarity solution valid for $\zeta \ll 1$, $j=0$ for the 2D case (a,b) and for the axisymmetric case ($j=1$) with $R_0=0.1$ (c,d), with $\Lambda=0$ (a,c) and $\Lambda=1$ (b,d). $Pr=0.7$, $\theta_f=0$.

Figures 5(a) and 6(a) show some vertical profiles of the radial velocity as ζ increases for $j=0$ and $j=1$ with $R_0=0.1$, respectively. Also shown (5b and 6b) are these velocity profiles scaled with the self-similar variables in (4.2), showing that they collapse into a single profile as r increases. To better appreciate that the numerical solutions tend to Glauert's similarity solution far away from the jet exit, we also plot in figures 5(c,d) and 6(c,d) the maximum radial velocity and its location conveniently scaled, $u_{max}r^{(j+1/2)}$ and $y_{max}r^{(j+3/2)/2}$, as functions of r. Note that the similarity solution is reached faster as r increases in the axisymmetric case ($j=1$, figure 6), obviously due to the radial divergence of the flow. Finally, figure 7 shows the scaled skin friction $c_f r^{(3j+5/2)/2}$ as a function of r for the same cases. All these quantities tend to constant values as r increases, corroborating that Glauert's self-similar solution is reached. The same happens for other values of Pr and $\theta_f \neq 0$.

4.3. *Results for* $\Lambda > 0$

Figures 8 and 9 shows some vertical profiles of the horizontal velocity when $\Lambda=0.1$ (with $Pr=0.7$ and $\theta_f=0$) for both the 2D case and the axisymmetric flow (with $R_0=0.1$), respectively. It is observed that the velocity profiles collapse far from the jet exit to the similarity solution described in § 3 (when scaled appropriately). The same happens for the temperature profiles. But it is more instructive to show the local friction coefficient and Nusselt number written in the similarity variable (3.14), (3.15). This is done in figures 10 and 11, respectively, for $Pr=0.7$, not only for the cases of figures 8 and 9, but for some other values of Λ, θ_f, and R_0. As predicted in § 3, the curves tend to asymptotic values as r increases which are independent of Λ, θ_f and R_0 (in the axisymmetric case), depending only on j (when Pr is fixed). Note that

https://doi.org/10.1017/jfm.2016.124 Published online by Cambridge University Press

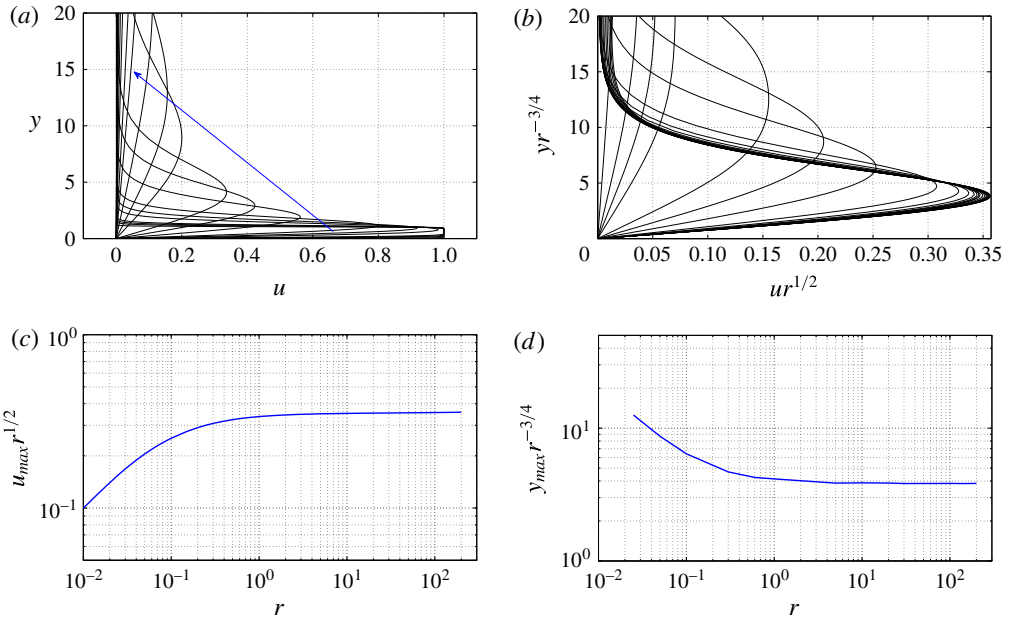


FIGURE 5. (Colour online) (*a*) Vertical profiles of the horizontal velocity u at different values of ζ, as indicated below, for $j = 0$, $\Lambda = 0$, $Pr = 0.7$ and $\theta_f = 0$. (*b*) The same profiles scaled with Glauert's similarity variables (4.2). (*c*,*d*) Maximum of u scaled with (4.2), and the scaled vertical location of this maximum, as functions of r. (*a*) $\zeta = 0.0003$, 0.0014, 0.0028, 0.005, 0.025, 0.05, 0.1, 0.3, 0.6, 1, 3, 5, 10, 20, 30, 50, 70, 100, 130, 160, 200, increasing in the direction of the arrow.

these asymptotes are reached much faster in the axisymmetric case than in the 2D flow. These figures include two cases with an inlet jet temperature different from the ambient temperature, $\theta_f = 0.5$, one case for a 2D flow and the other one for a radial flow. In spite of the fact that the inlet conditions are very different, particularly for the temperature (see, for instance, figure 12, where we compare the temperature profiles for $\theta_f = 0$ and $\theta_f = 0.5$ in the 2D flow), both flows tend to the same corresponding similarity solution as r increases, that only depends on j when Pr is fixed. Note that $c_f(r)$ is hardly modified by the different inlet temperatures, especially for $j = 1$ (figure 10), but $Nu(r)$ for $\theta_f = 0$ and $\theta_f = 0.5$ are quite different (figure 11) due to the very different initial temperature profiles (see figure 12), until reaching the common asymptote. Similar behaviours are found for inlet temperatures higher than the ambient temperature, $\theta_f > 1$, not shown.

Figures 13–14 show c_f and Nu for different values of Pr at selected values of the other parameters. In agreement with the analytical results in § 3, the asymptotic value of the friction coefficient for $r \gg 1$ decreases with increasing Pr, all the remaining parameters the same, being larger for the 2D flow ($j = 0$) than for the radial flow ($j = 1$). In contrast, the Nusselt number increases with Pr, being larger for the axisymmetric case than for the 2D flow.

5. Summary and conclusion

A similarity solution for the wall jet over a heated horizontal plate at constant temperature that takes into account the coupling of temperature and velocity fields

https://doi.org/10.1017/jfm.2016.124 Published online by Cambridge University Press

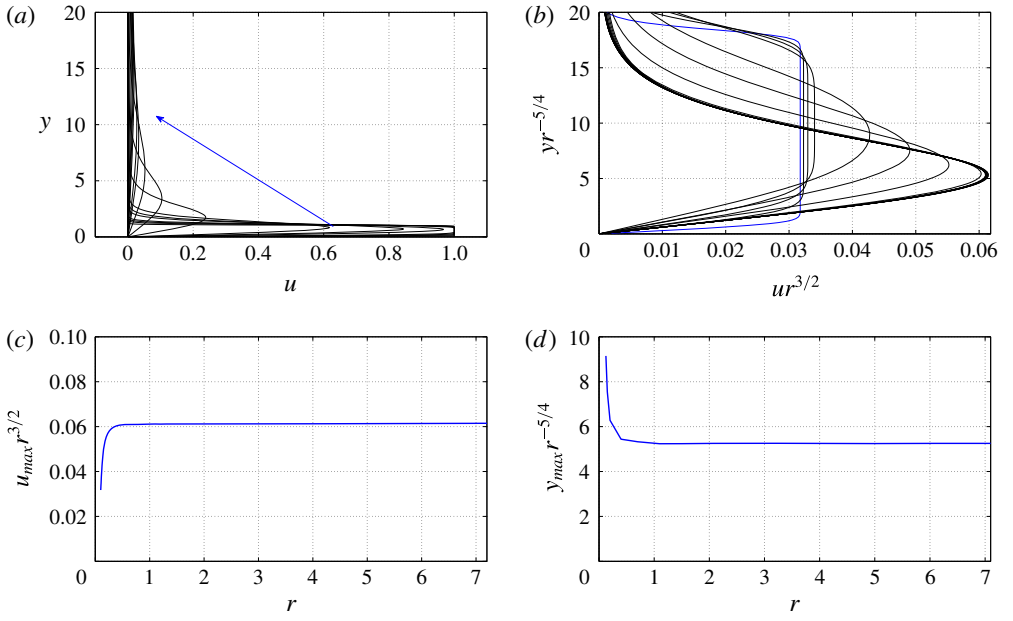


FIGURE 6. (Colour online) As in figure 5, but for $j=1$ with $R_0=0.1$: (*a*) $\zeta=0.0003$, 0.0014, 0.0028, 0.005, 0.025, 0.05, 0.1, 0.3, 0.6, 1, 1.4, 1.6, 2.1, 2.3, 2.5, 2.9, 3.6, 4.8, 6, 7, increasing in the direction of the arrow.

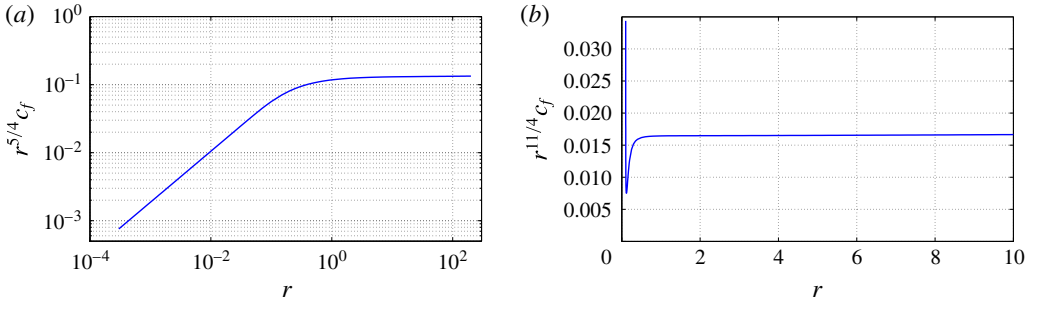


FIGURE 7. (Colour online) Evolution with r of the skin friction at the wall scaled according to (4.4) for the same cases plotted in figures 5 and 6: $\Lambda=0$, $Pr=0.7$, $\theta_f=0$, for $j=0$ in (*a*), and for $j=1$ with $R_0=0.1$ in (*b*).

through buoyancy has been described. For a given temperature difference between the plate and the ambient, T_0-T_a, a vertical scale length δ, and a characteristic horizontal velocity U, this coupling is quantified by the dimensionless parameter $\Lambda=\beta g\delta(T_0-T_a)/U^2=Gr/Re^2$, where Re and Gr are the corresponding Reynolds and Grashof numbers, respectively. Λ is also equivalent to the inverse of a Froude number. For $\Lambda=0$ one has the well-known Glauert's (1956) similarity solution for a wall jet without buoyancy. But this solution is qualitatively very different from the one found here for $\Lambda>0$ in two main aspects. First, Glauert's similarity variable is $\tau_G\propto y/r^{(j+3/2)/2}$, while for $\Lambda\neq0$ we find $\tau\propto y/r^{2/5}$, both for the 2D flow ($j=0$) and for the axisymmetric, or radially spreading, flow ($j=1$). Thus, the basic structure of

https://doi.org/10.1017/jfm.2016.124 Published online by Cambridge University Press

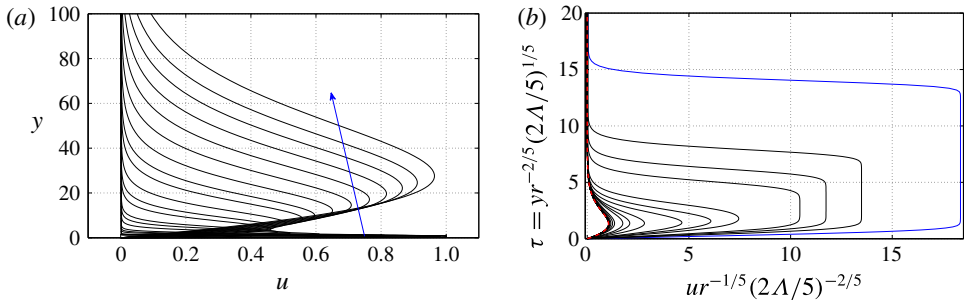


FIGURE 8. (Colour online) (*a*) Vertical profiles of u at different values of ζ, as indicated below, for $j = 0$, $\Lambda = 0.1$, $Pr = 0.7$ and $\theta_f = 0$. (*b*) The same profiles scaled with the similarity variables (3.9)–(3.10). Also included in (*b*) with a dashed (red) line is $f'(\tau)$ for $j = 0$ and $Pr = 0.7$ from figure 2. (*a*) $\zeta = 0.0003$, 0.0014, 0.0028, 0.005, 0.025, 0.05, 0.1, 0.3, 0.6, 1, 3, 5, 10, 20, 30, 50, 80, 120, 170, 230, 300, 400, increasing in the direction of the arrow.

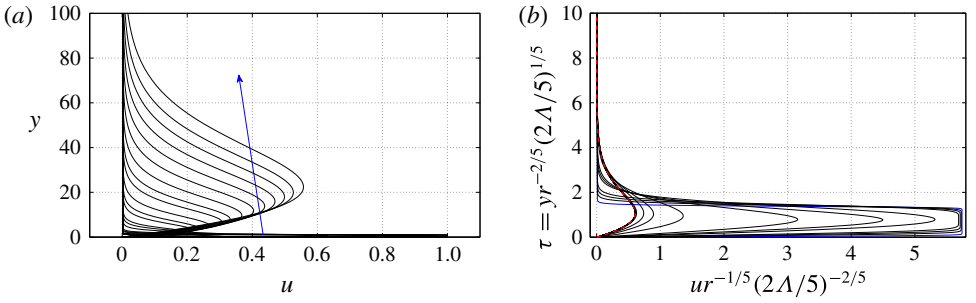


FIGURE 9. (Colour online) As in figure 8, but for the axisymmetric case ($j = 1$) with $R_0 = 0.1$: (*a*) $\zeta = 0.0003$, 0.0014, 0.0028, 0.005, 0.025, 0.05, 0.1, 0.3, 0.6, 1, 3, 5, 10, 20, 30, 50, 80, 120, 170, 230, 300, 400, increasing in the direction of the arrow.

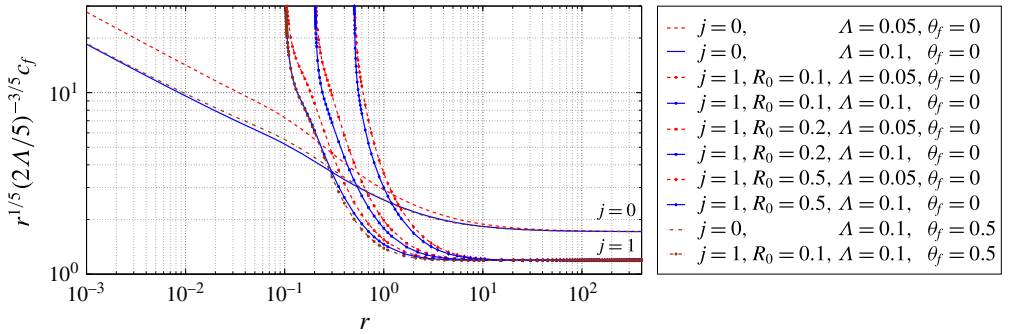


FIGURE 10. (Colour online) Evolution with r of the friction coefficient at the wall c_f scaled according to (3.14) for several values of the parameters, as indicated, all with $Pr = 0.7$.

the similarity flow is the same for the planar and the radial flow, and very different from the two distinct flow structures in Glauert's similarity solution. Second, the

https://doi.org/10.1017/jfm.2016.124 Published online by Cambridge University Press

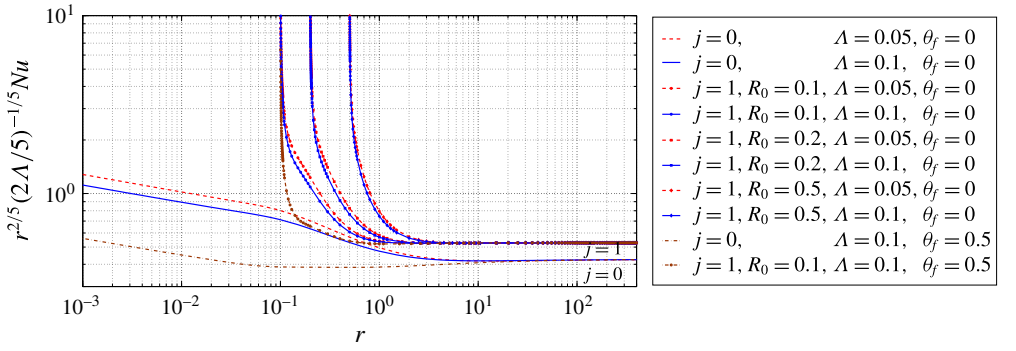


FIGURE 11. (Colour online) Evolution with r of the local Nusselt number scaled according to (3.15) for several values of the parameters, as indicated, all with $Pr=0.7$.

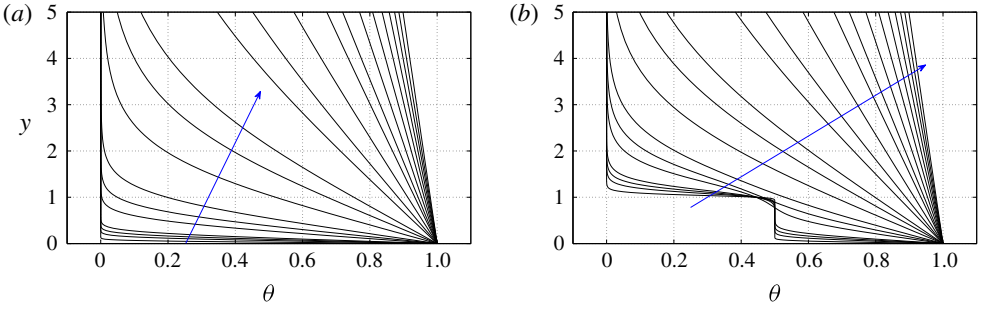


FIGURE 12. (Colour online) Vertical profiles of θ at different values of ζ, as indicated below, for $j=0$, $\Lambda=0.1$, $Pr=0.7$, $\theta_f=0$ (*a*) and $\theta_f=0.5$ (*b*): (*a*,*b*) $\zeta=0.0003$, 0.0014, 0.0028, 0.005, 0.025, 0.05, 0.1, 0.3, 0.6, 1, 3, 5, 10, 20, 30, 50, 80, 120, 170, 230, 300, 400, increasing in the direction of the arrow.

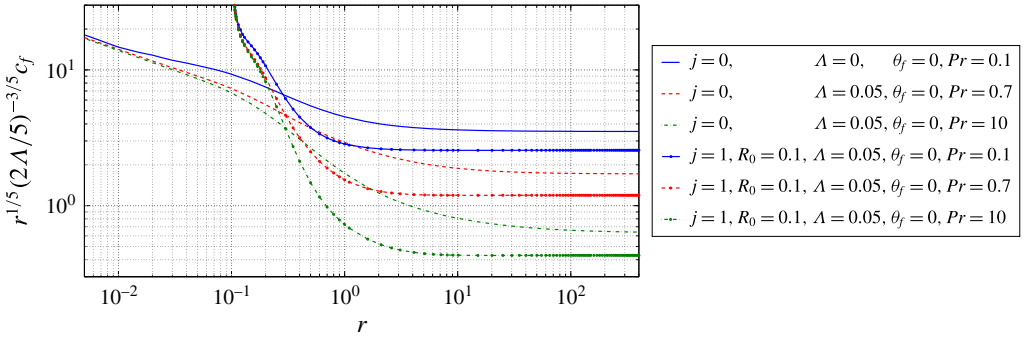


FIGURE 13. (Colour online) Evolution with r of the friction coefficient at the wall c_f scaled according to (3.14) for several values of Pr at selected values of the remaining parameters, as indicated.

radial or horizontal velocity increases with r as $u \propto r^{1/5}$, both for the 2D flow and for the axisymmetric flow, while in Glauert's solution it decays as $u_G \propto r^{-(j+1/2)}$. In addition, the radial dependence of the temperature field differs from the one associated

https://doi.org/10.1017/jfm.2016.124 Published online by Cambridge University Press

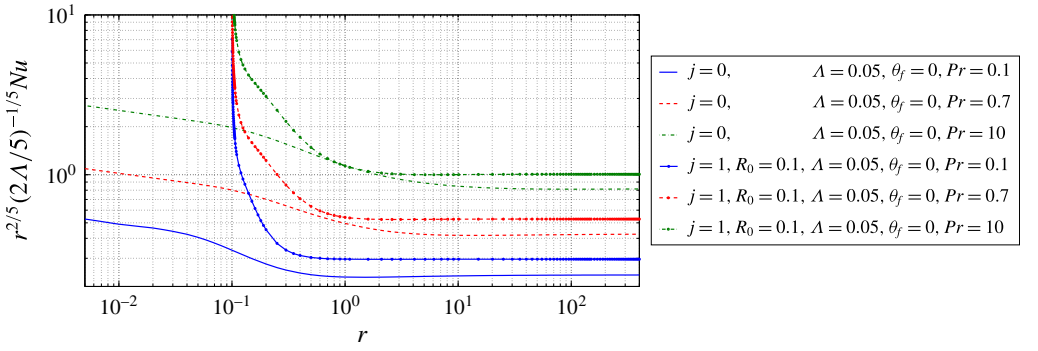


FIGURE 14. (Colour online) Evolution with r of the local Nusselt number scaled according to (3.15) for several values of Pr at selected values of the other parameters, as indicated.

to Glauert's flow. The similarity solution described here is also qualitatively different from the one found by Stewartson (1958) for the purely free convection flow over a horizontal plate because no characteristic velocity exists in this last problem, so that no equivalent to the parameter Λ, or to a Froude number, exists. Also, only the two-dimensional ($j=0$) flow was considered by Stewartson.

Parameter Λ is embedded into the similarity solution, so that the dependence with Λ of the velocity and temperature fields and, consequently, of the skin friction and heat flux at the wall, are given explicitly. In particular, the friction coefficient and Nusselt number behave as

$$c_f \propto \Lambda^{3/5} r^{-1/5}, \quad Nu \propto \Lambda^{1/5} r^{-2/5}, \tag{5.1a,b}$$

both for the 2D flow and for the axisymmetric flow. Simple correlations for the proportionality constants in (5.1) as functions of the Prandtl number Pr are given for $j=0$ and $j=1$.

To check the validity of this similarity solution we have solved numerically the boundary layer flow emerging radially with uniform velocity U and temperature T_f from a circular slot of radius r_0 and height δ over a plate at constant temperature T_0 and into an ambient fluid at rest with temperature T_a. In addition to Λ, the problem is governed by the dimensionless parameters Pr, θ_f ($\neq 0$ if $T_f \neq T_a$), and, in the axisymmetric case, R_0, related to r_0. A self-similar solution valid near the jet exit is also provided in this work, which in addition serves to initiate the numerical integration of the boundary layer equations towards the far-field solution. We have checked that the similarity solution is reached far from the jet exit for all the values of j, Pr, θ_f and R_0 investigated, provided that $\Lambda > 0$, i.e. $T_0 > T_a$. For $\Lambda < 0$ (cooled plate), the far-field similarity solution does not exist, as is clear from its structure (e.g. (5.1)), and as previously reported in related mixed-convection flows over a cooled plate at constant temperature (Schneider & Wasel 1985; Steinrück 1994, 1995; Higuera 1997). We find numerically that the boundary layer solution for $\Lambda < 0$ always breaks down at a finite streamwise distance from the jet exit because reverse flow is originated within the boundary layer due to the adverse pressure gradient induced by buoyancy when $\Lambda < 0$, and a similarity solution is never attained. In all the cases with $\Lambda < 0$ that we have explored numerically, reverse flow inside the boundary layer

https://doi.org/10.1017/jfm.2016.124 Published online by Cambridge University Press

is first originated at some distance from the wall, so that the skin friction c_f does not vanish at, or just before, the failure of the numerical scheme. On the other hand, no terminal singularity of the skin friction like that described by Daniels (1992) and Daniels & Gargaro (1993) for a horizontal insulated surface has been found in the present problem. We suspect that in the axisymmetric case ($j = 1$), and for sufficiently small R_0, the boundary layer solution also breaks down as r increases above a threshold value of $\Lambda > 0$, and the similarity solution is not reached, but we have not explored this possibility in the present work. For $\Lambda = 0$ Glauert's similarity solution is recovered for any set of values of the remaining parameters investigated.

Appendix A. Approximate solution near the jet exit

An approximate solution for small $\zeta \equiv r - jR_0$ which is of interest not only from a theoretical point of view, but also to start the numerical integration of the parabolic equations (2.2)–(2.4), is obtained here. At its lowest order in powers of ζ this solution is composed by the self-similar Blasius solution near $y = 0$ plus the self-similar solution for a plane half-jet near $y = 1$ (see, e.g. Schlichting & Gersten 2000). In particular, for $\zeta \ll 1$ and $\zeta \ll R_0$ (in the axisymmetric case), one may write (3.1), in first approximation, as

$$u \simeq \left(1 - j\frac{\zeta}{R_0}\right)\frac{\partial \psi}{\partial y}, \quad v \simeq -\left(1 - j\frac{\zeta}{R_0}\right)\frac{\partial \psi}{\partial \zeta}, \tag{A 1a,b}$$

where the constant R_0^{-j} has been absorbed into ψ. As $\zeta \to 0$, $\sqrt{\zeta}\,\psi$ and θ are functions of Blasius' similarity variable

$$\tau_0 = \frac{y}{\sqrt{\zeta}}, \tag{A 2}$$

for $y \ll 1$, while they are functions of

$$\tau_1 = \frac{y-1}{\sqrt{\zeta}}, \tag{A 3}$$

for $|y - 1| \ll 1$ (Lessen 1949). Thus, close to $y = 0$ and $y = 1$ one may use the following expansions for $\zeta \ll 1$:

$$\psi_i = \zeta^{1/2} f_{i0}(\tau_i) + \zeta f_{i1}(\tau_i) + \cdots, \tag{A 4}$$

$$\theta_i = \theta_{i0}(\tau_i) + \zeta^{1/2}\theta_{i1}(\tau_i) + \cdots, \tag{A 5}$$

with $i = 0$ and $i = 1$, respectively. Substituting these expansions into (2.3)–(2.4) one obtains, for the two first terms in the expansion,

$$f_{i0}''' + \tfrac{1}{2} f_{i0} f_{i0}'' = 0, \tag{A 6}$$

$$\theta_{i0}'' + \frac{Pr}{2} f_{i0}\,\theta_{i0}' = 0, \tag{A 7}$$

$$f_{i1}''' + \frac{1}{2} f_{i0} f_{i1}'' - \frac{1}{2} f_{i0}' f_{i1}' + f_{i0}'' f_{i1} = -\frac{\Lambda}{2}\left[\tau_i(\theta_{i0} - \theta_f) + \int_{\tau_i}^{\infty} \theta_{i0}\,\mathrm{d}\tau_i\right], \tag{A 8}$$

$$\theta_{i1}'' + Pr\left(f_{i1}\theta_{i0}' + \tfrac{1}{2} f_{i0}\theta_{i1}' - \tfrac{1}{2} f_{i0}'\theta_{i1}\right) = 0, \tag{A 9}$$

https://doi.org/10.1017/jfm.2016.124 Published online by Cambridge University Press

for $i = 0$ and $i = 1$, where the primes denote differentiation with respect to the corresponding τ_i. These equations have to be solved with the following boundary conditions:

for $i = 0$,

$$f_{00}(0) = f'_{00}(0) = 0, \quad \theta_{00}(0) = 1, \quad f'_{00}(\infty) = 1, \quad \theta_{00}(\infty) = \theta_f, \tag{A 10a–d}$$

$$f_{01}(0) = f'_{01}(0) = \theta_{01}(0) = 0, \quad f'_{01}(\infty) = \theta_{01}(\infty) = 0; \tag{A 11a,b}$$

for $i = 1$,

$$f_{10}(\tau_1 \to -\infty) \to f_{00}(\infty) + \tau_1, \quad f'_{10}(-\infty) = 1, \quad \theta_{10}(-\infty) = \theta_f, \tag{A 12a–c}$$

$$f'_{10}(\infty) = 0, \quad \theta_{10}(\infty) = 0, \tag{A 13a,b}$$

$$f_{11}(-\infty) = f_{01}(\infty), \quad f'_{11}(-\infty) = \theta_{11}(-\infty) = 0, \quad f'_{11}(\infty) = \theta_{11}(\infty) = 0. \tag{A 14a–c}$$

First one solves the equations for τ_0, and then those for τ_1 using the obtained values $f_{00}(\infty)$ and $f_{01}(\infty)$ in the boundary conditions (A 13)–(A 14).

Note that with just these two terms in the expansions, first-order buoyancy effects are taken into account through the second term, but one does not see the radial divergence of the flow in the axisymmetric case. This radial effect enters at the next order (third term) in the expansions (A 4)–(A 5) in powers of ζ (Fernandez-Feria *et al.* 2014). But the above two terms are enough to start with accuracy the numerical integration of equations (2.2)–(2.11*a*,*b*). Actually, one uses as initial conditions a composite self-similar solution, which is obtained adding the terms for $i = 0$ and for $i = 1$ and subtracting the common terms as $\tau_0 \to \infty$ and $\tau_1 \to -\infty$, respectively. In particular, we use the following initial conditions at a given $r_{in} = \zeta_{in} + jR_0$, $\zeta_{in} \ll 1$, to solve (2.2)–(2.11*a*,*b*) numerically:

$$u_{in}(y) \equiv u(r_{in}, y) = f'_{00}(\tau_{0in}) + \zeta_{in}^{1/2} f'_{01}(\tau_{0in}) + f'_{10}(\tau_{1in}) + \zeta_{in}^{1/2} f'_{11}(\tau_{1in}) - 1, \tag{A 15}$$

$$\begin{aligned} v_{in}(y) \equiv v(r_{in}, y) = {} & -\tfrac{1}{2}\zeta_{in}^{-1/2}\left[f_{00}(\tau_{0in}) - \tau_{0in} f'_{00}(\tau_{0in})\right] - f_{01}(\tau_{0in}) + \tfrac{1}{2}\tau_{0in} f'_{01}(\tau_{0in}) \\ & - \tfrac{1}{2}\zeta_{in}^{-1/2}\left[f_{10}(\tau_{1in}) - \tau_{1in} f'_{10}(\tau_{1in})\right] - f_{11}(\tau_{1in}) + \tfrac{1}{2}\tau_{1in} f'_{11}(\tau_{0in}) + \tfrac{1}{2}\zeta_{in}^{-1/2} f_{00}(\infty) \\ & + f_{01}(\infty), \end{aligned} \tag{A 16}$$

$$\theta_{in}(y) \equiv \theta(r_{in}, y) = \theta'_{00}(\tau_{0in}) + \zeta_{in}^{1/2}\theta'_{01}(\tau_{0in}) + \theta'_{10}(\tau_{1in}) + \zeta_{in}^{1/2}\theta'_{11}(\tau_{1in}) - \theta_f, \tag{A 17}$$

where $\tau_{0in} = y/\sqrt{\zeta_{in}}$ and $\tau_{1in} = (y-1)/\sqrt{\zeta_{in}}$. Figure 15 shows these initial profiles for $\zeta_{in} = 2 \times 10^{-3}$ in some particular cases. Since the radial divergence effect is not accounted for in the present approximation with just two terms in the expansions (A 4)–(A 5), these initial profiles are independent of j and, consequently, of R_0. Note also than for $\Lambda = 0$ the second correction in the expansion for $\zeta \ll 1$ vanish, so that the continuous lines in figure 15 for $\Lambda = 0$ coincide with the lowest order of the expansion for $\Lambda \neq 0$. Finally, it is worth mentioning that v is always negative as $y \to \infty$. This is a consequence of the fact that both u and θ vanish as $y \to \infty$: if $v_\infty(r) \equiv v(r, y \to \infty)$, the solution of (2.4) as $y \to \infty$ that satisfies the boundary condition at infinity behaves as $\theta \sim C(r)\exp[Pr\, v_\infty y]$, implying that $v_\infty(r) < 0$ for any r. Similarly, (2.3) implies that the leading term of u as $y \to \infty$ behaves as $u \sim$

https://doi.org/10.1017/jfm.2016.124 Published online by Cambridge University Press

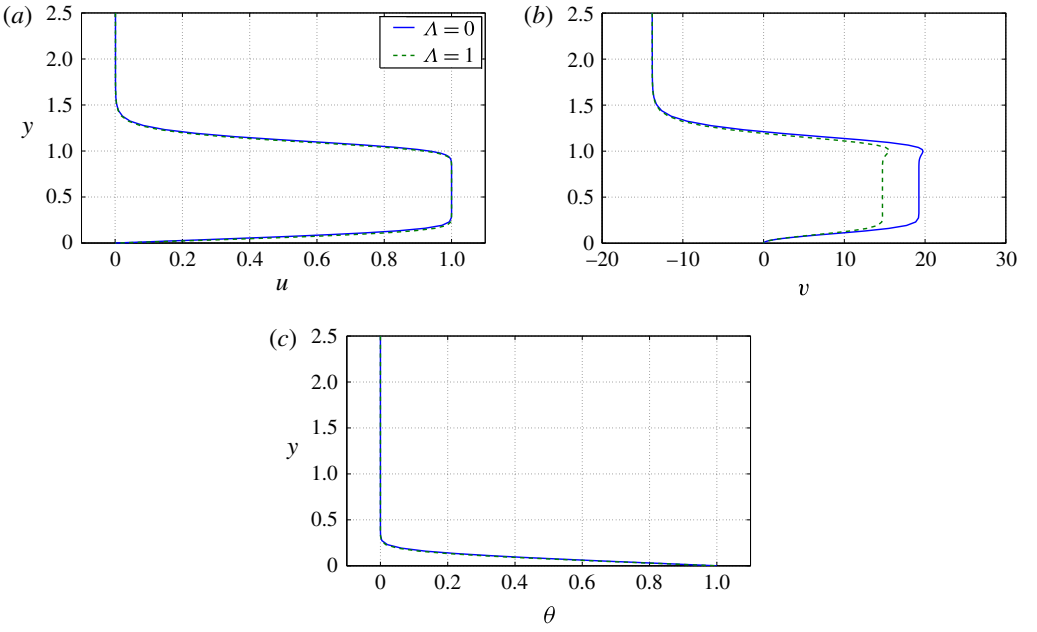


FIGURE 15. (Colour online) Vertical profiles of u (a), v (b), and θ (c), given by (A 15)–(A 17), at $\zeta_{in} = 2 \times 10^{-3}$ for $Pr = 0.7$, $\theta_f = 0$ and two values of Λ, as indicated.

$K_1(r)y \exp[Pr\, v_\infty y]$ or as $u \sim K_2(r) \exp[v_\infty y]$, depending on whether Pr is larger or smaller than unity, respectively, with $K_1(r)$ related to $C(r)$. In both cases $v_\infty(r)$ should be negative for any r.

REFERENCES

AFZAL, N. & HUSSAIN, T. 1984 Mixed convection over a horizontal plate. *Trans. ASME J. Heat Transfer* **106**, 240–241.

BOYD, J. P. 2000 *Chebyshev and Fourier Spectral Methods*, 2nd edn. Dover.

DANIELS, P. G. 1992 A singularity in thermal boundary-layer flow on a horizontal surface. *J. Fluid Mech.* **242**, 419–440.

DANIELS, P. G. & GARGARO, R. J. 1992 Numerical and asymptotic solutions for the thermal wall jet. *J. Engng Maths* **26**, 493–508.

DANIELS, P. G. & GARGARO, R. J. 1993 Buoyancy effects in stably stratified horizontal boundary-layer flow. *J. Fluid Mech.* **250**, 233–251.

DENIER, J. P., DUCK, P. W. & LI, J. 2005 On the growth (and suppression) of very short-scale disturbances in mixed froce-free convection boundary layers. *J. Fluid Mech.* **526**, 147–170.

DESWITA, L., NAZAR, R., ISHAK, A., AHMAD, R. & POP, I. 2010 Similarity solutions for mixed convection boundary-layer flow over a permeable horizontal plate. *Appl. Maths Comput.* **217**, 2619–2630.

FERNANDEZ-FERIA, R. & ORTEGA-CASANOVA, J. 2014 A pseudospectral based method of lines for solving integro-differential boundary-layer equations. *Appl. Maths Comput.* **242**, 388–396.

FERNANDEZ-FERIA, R., DEL PINO, C. & FERNANDEZ-GUTIERREZ, A. 2014 Separation in the mixed convection boundary-layer radial flow over a constant temperature horizontal plate. *Phys. Fluids* **26**, 103603.

GILL, W. N. & DEL CASAL, E. 1962 A theoretical investigation of natural convection effects in forced horizontal flows. *AIChE J.* **8**, 513–518.

https://doi.org/10.1017/jfm.2016.124 Published online by Cambridge University Press

GLAUERT, M. B. 1956 The wall jet. *J. Fluid Mech.* **1**, 625–643.

HIGUERA, F. J. 1997 Opposing mixed convection flow in a wall jet over a horizontal plate. *J. Fluid Mech.* **342**, 355–375.

LEAL, L. G. 1973 Combined forced and free convection heat transfer from a horizontal flat plate. *Z. Angew. Math. Phys.* **24**, 20–42.

LESSEN, M. 1949 On the stability of the free laminar boundary layer between parallel streams. *NACA Tech. Rep*. NACA-R-979.

SCHLICHTING, H. & GERSTEN, K. 2000 *Boundary Layer Theory*, 8th edn. Springer.

SCHNEIDER, W. 1979 A similarity solution for the combined forced and free convection flow over a horizontal plate. *Intl J. Heat Mass Transfer* **22**, 1401–1406.

SCHNEIDER, W. & WASEL, M. G. 1985 Breakdown of the boundary-layer approximation for mixed convection above a horizontal plate. *Intl J. Heat Mass Transfer* **28**, 2307–2313.

SPARROW, E. M., EICHHORN, R. & GREGG, J. L. 1959 Combined forced and free convection in a boundary-layer flow. *Phys. Fluids* **2**, 319–328.

STEINRÜCK, H. 1994 Mixed convection over a cooled horizontal plate: non-uniqueness and numerical instabilities of the boundary-layer equations. *J. Fluid Mech.* **278**, 251–265.

STEINRÜCK, H. 1995 Mixed convection over a horizontal plate: self-similar and connecting boundary-layer flows. *Fluid Dyn. Res.* **15**, 113–127.

STEWARTSON, K. 1958 On the free convection from a horizontal plate. *Z. Angew. Math. Phys.* **IXa**, 276–282.

https://doi.org/10.1017/jfm.2016.124 Published online by Cambridge University Press